JOURNAL OF MATERIALS SCIENCE 37 (2002) 825–834

Influence of humidity on the cracking patterns formed during the drying of sol-gel drops

B. D. CADDOCK, D. HULL
Department of Engineering, University of Liverpool, Liverpool L69 3BX, UK

Optical microscopy has been used to study the sequence of events associated with drying of a silica-based sol-gel. Drops of sol containing 50 wt% silica were deposited on glass slides and dried in cells containing sulphuric acid as a drying agent. The drops, on the slide, were about 3.5 mm in diameter and before the onset of drying had a spherical cap shape. At the start of drying the rim of the drops became pinned to the glass surface. The humidity of the drying environment had a strong effect on shrinkage within the drop and the processes that occurred during drying. In very dry environments evaporation occurred primarily from the edges of the drop and resulted in a radial concentration gradient in the gel. Shrinkage resulted in a pattern of radial cracks that spread from the outside in a direction orthogonal to the iso-concentration profiles. Cracking was preceded by shear deformation. Drying was more uniform in humid environments and occurred from both the rim and the top surface of the drop. Wrinkling of the skin of gel that formed on the surface of the drop was followed by radial and circumferential cracking, except in very humid environments. The results are attributed to the influence of the radius of curvature of the drop surface on the rate of evaporation and the relative rates of flow and diffusion in the drying sol-gel.

1. Introduction

In a previous paper [1] we describe experiments to simulate the formation of shrinkage-driven cracks during the solidification of basaltic lava flows. We used a sol-gel formed from a 50% (by weight) dispersion of silica particles in water. The complex cracking patterns in basaltic rock formations were explained by assuming that cracks nucleate and grow in directions normal to the principal tensile stresses in the cooling lava. These directions are parallel to the thermal gradients so that the arrangement and shape of the cracks depend on the distribution of the cooling isotherms. The thermal gradients in cooling lava were simulated by the water concentration gradients in the drying sol-gel. Experimental methods were developed to vary the direction of the concentration gradients and so generate cracking patterns in the sol-gel that matched those found in rock formations.

One of the patterns that we examined during this earlier work (not reported in [1]) was that formed in an open sessile drop of sol-gel resting on the surface of a microscope slide. The cracking pattern consisted of an array of approximately equally spaced radial cracks that initiated at the rim of the drop and grew inwards at a rate determined by the rate of drying. During this study evidence was obtained that the cracking pattern was influenced by the rate of drying indicating that the stresses that developed in the drop also depended on the rate of drying. The nucleation of cracks at the rim of the drop suggested that drying of the sol occurred preferentially in this region.

A number of processes are involved during drying. For an isolated spherical drop of pure water the rate of evaporation is related to the radius of curvature of the surface of the drop, r, by Maxwell's equation [2]

$$I = 4\pi r D(c_o - c_\infty) \tag{1}$$

where I is the total rate of evaporation (total mass loss per unit time), D is the water vapour diffusion coefficient and C_o and C_∞ are the water vapour concentrations at the surface of the drop and infinity respectively. It follows that, at any given temperature, the evaporative flux or specific evaporation rate, J (mass loss per unit time per unit area) is inversely proportional to the drop radius.

$$J = \text{constant}/r \tag{2}$$

Experiments by Peiss [3] have confirmed the strong effect of the radius of curvature of the surface on the evaporation rate.

A drop of water on a flat surface spreads out and assumes the shape of a spherical cap, (Fig. 1), providing it is sufficiently small that the effects of gravity are insignificant [4, 5]. The drop shrinks when evaporation occurs, as illustrated in Fig. 2a, providing the contact line between the rim of the drop and the solid surface is not pinned. When the edge of the drop is pinned evaporation results in a drop with a different shape, Fig. 2b. Whether or not the drop is pinned it is established [6, 7] that the evaporative flux is greatly enhanced at the rim

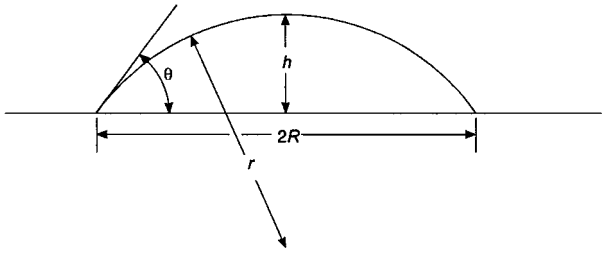

Figure 1 Shape of a liquid drop on a flat surface.

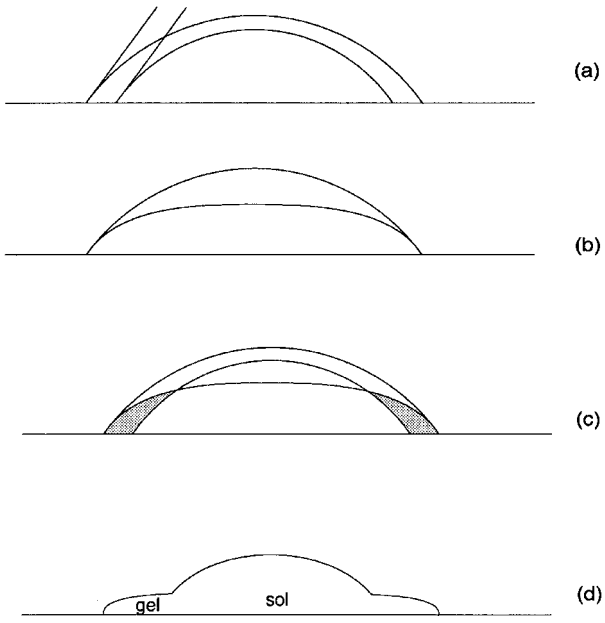

Figure 2 Change of shape of drop resulting from evaporation: (a) shrinkage of drop by evaporation without pinning at the rim, (b) shrinkage of a pinned drop, (c) redistribution of liquid associated with difference between an unpinned drop and a pinned drop, and (d) development of a foot in region of gel formation.

of the drop. The process has been modelled [6] by analogy with an equivalent electrostatic problem in which the dominant feature is the sharp discontinuity at the rim. The diagrams in Fig. 2 also demonstrate the requirement for a second process in drying involving the flow of liquid from the centre of the drop to the outer regions. This is particularly evident for a drop pinned at the rim. The changes in shape (Fig. 2b and c) result in a redistribution of liquid.

This additional effect is particularly important in drops of liquid containing fine dispersions of solids, as in sol-gels. Evidence for flow was presented by Deegan *et al*. [6] and was observed in our earlier sol-gel studies [1]. The flow of liquid to the outer rim of the drop, and preferential drying at the rim, leads to drying of the sol in this region. The sol changes progressively to a rigid gel. It seems likely that this process promotes the pinning of the rim. Parisse and Allain [7] have demonstrated that the profile of partially dried sol-gel drops develops a characteristic shape, as shown in Fig. 2d. The gelled rim is called a foot and has a smaller radius of curvature than the original drop. Note that, since the gelled material is highly porous, transport of water to the outer regions of the drop continues through the gel.

A third factor influencing the sequence of events during drying of sol-gels is the equilibrium requirement that the water concentration should be uniform throughout the drop. There are, therefore, three distinct time dependent effects associated with drying: (1) evaporation, (2) transport of water associated with the change of shape of the drop (a hydrodynamic flow process), and (3) transport of water to maintain an equilibrium concentration of water (a diffusive flow process). The progressive change from a sol to a gel and the movement of the sol-gel interface then depends on the relevant contributions of these three factors. Equally, the development of shrinkage stresses and the growth of cracks also depend on these factors. This paper describes experiments in which the evaporative flux is controlled by the humidity of the drying environment so generating a range of drying profiles and cracking patterns.

2. Experimental

The same commercial aqueous silica sol, described in our previous paper, was used in this work. It is produced by Du Pont and marketed as Ludox TM-50. The sol is a mobile liquid consisting of 50 wt% silica dispersed as particles, about 30 nm diameter, in water. A small amount of alkali is dissolved in the water to stabilise the colloidal suspension. The sol is stable whilst stored at room temperature in a sealed container but gels rapidly when allowed to evaporate in air.

Drops of sol, deposited on glass slides, were dried in sealed containers in the presence of sulphuric acid, of various concentrations, to control the relative humidity in the container. The experimental arrangement is illustrated in Fig. 3. The container or cell is a 95 mm diameter Petri dish. The drop of sol rests on a glass slide that is supported on two glass blocks. The two halves of the Petri dish are sealed with grease. Inside the cell there are two rectangular ceramic dishes containing sulphuric acid. Direct observation of the sequence of events associated with drying and cracking of the sol-gel was achieved by placing the cell on the stage of a Nikon Optiphot optical microscope and viewing in both transmitted and reflected light using a long focal

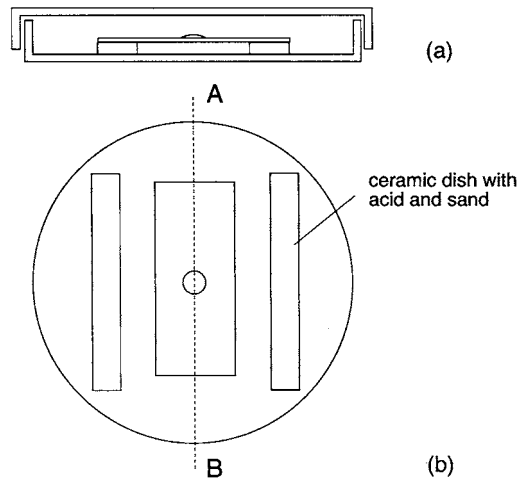

Figure 3 Experimental arrangement for transmitted light microscope observations of progress of drying in a 95 mm diameter Petri dish: (a) section through dish at AB showing Ludox TM-50 drop on a glass slide, (b) plan view of Petri dish.

TABLE I Comparison of equilibrium vapour pressures of water vapour and SO_3 over aqueous sulphuric acid at 20°C

Acid content weight %	Equilibrium vapour pressure of SO_3 (mbar)	Equilibrium vapour pressure of water (mbar)
80	2.80E-12	0.12
50	6.21E-19	8.02
20	3.94E-23	20.5
10	2.78E-24	22.3

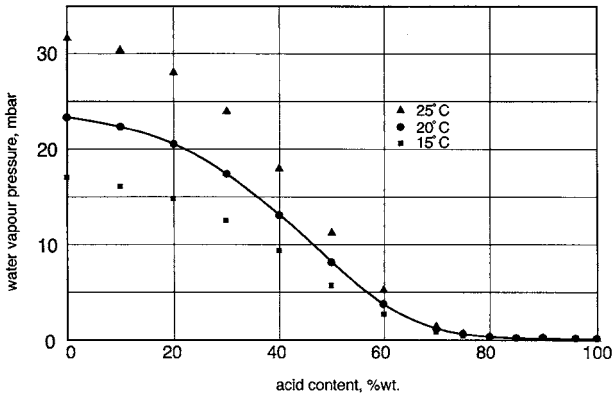

Figure 4 Variation of equilibrium water vapour pressure over aqueous sulphuric acid at 15, 20 and 25°C.

length objective lens with monochromatic light. The contrast effects observed in the microscope depended on the aperture settings.

Concentrated sulphuric acid is a strong desiccant. The equilibrium partial pressures of water over aqueous sulphuric acid are shown in Fig. 4 at three temperatures. The drying experiments were carried out at 20+/−2°C with sulphuric acid concentrations in the range 6 to 65 wt% acid so that the effective range of water vapour pressures was 0 to 23 mbar. It is highly unlikely in the time-scale of most of the experiments that these equilibrium values were achieved during drying. In practice the water vapour pressures in the cell are higher than the equilibrium values until drying stops. Thus, it was only possible to change the water vapour pressure, and hence the drying rates in a qualitative way. The vapour pressures of SO_3 at 20°C for different concentrations of sulphuric acid are given in Table I. Even with the most concentrated acids the SO_3 vapour pressure is 13 orders of magnitude lower than that of water so that it is highly unlikely that this vapour influenced the drying process.

Drops of Ludox sol were produced using a Gilson pipette. A fixed volume was dispensed using a special jig to produce drops on the glass slides with a diameter between 3.4 to 3.7 mm. This diameter was chosen for the purely practical reason that it is a size convenient for viewing and recording in the optical microscope. Super premium glass slides, that had been washed, cleaned and polished in manufacture, were used without any further preparatory treatments.

To follow the flow and diffusion of liquids in the sol-gel additional experiments were made by doping the Ludox sol, before depositing the drops on the slides, with small amounts of either a soluble dye (fluorescein) or a colloidal dispersion of graphite particles.

3. Results

3.1. Preliminary observations

The technique described in the previous section produced almost perfectly circular drops indicating that the surface of the glass was free from macroscopic heterogeneities. The outer rims of the drops were pinned to the glass so that the diameter of the drops remained the same size throughout drying until the very late stages when delamination from the glass occurred. Drying of single drops in closed cells gave uniform, concentric, drying profiles. Drying of multiple drops in closed cells and single drops drying in open cells produced non-uniform effects. Usually, the profiles were not concentric because the microclimate around the drops was influenced by the presence of adjacent drops and by air currents.

Using microgravimetric measurements it was found that 1.9 μl of Ludox TM-50, weighing 2.66 mg, produced a drop that spread to a circle 3.4 mm diameter on the glass slide. The contact angle, measured by an optical profile method, was $29 \pm 2°$. In the discussion later we show that before the onset of drying the radius of curvature of the surface of these drops is the same over the whole surface and that gravitational effects on the shape are minimal. In other words the surface forms as a spherical cap.

The changes in shape that accompany drying were followed indirectly by the changes in image contrast in the light microscope. In our previous paper [1] it was shown that drying in air resulted in the progressive growth of an array of cracks that were nucleated at the edges of drying sheets by local shrinkage. An equivalent effect was observed during fast drying of open drops. Fig. 5 shows a typical sequence, from the present work, for a drop dried in a cell containing a strong desiccant (oven-dried silica gel). In (a) the spherical cap-shaped drop has dried partially producing an outer rim or 'foot' of gel. The inner region is liquid sol that has retained its spherical shape. In (b) cracks, nucleated in the outer rim, have grown radially inwards and stopped at, or close to, the retreating gel-sol boundary. In (c) the sol-gel transformation is complete, the rim is still pinned, and a shrinkage hole has formed in the centre. The radial cracks extend to the hole and a circular secondary crack has formed close to the centre.

The time to the initiation of the first crack (cracking time) was used as a measure of the influence of humidity on the rate of drying and the cracking sequences. For drops dried in air and under very fast drying conditions at 20°C (Fig. 5) cracking started after 2 to 3 min. The effect of a range of humidities, expressed as equilibrium water vapour pressures, is shown in Fig. 6. It is important to emphasise, as mentioned earlier, that the water vapour pressures shown in the graph provide only an indication of the rate of drying since the humidity in the cells is changing continuously during the drying process. In cells containing less than 12% sulphuric acid (equilibrium vapour pressure of 22 mbar) the drops did not dry sufficiently for cracking to occur. This is a natural limit for the cracking data.

The results described below show that the processes associated with drying depend strongly on the drying rate. In separate experiments it was found that these

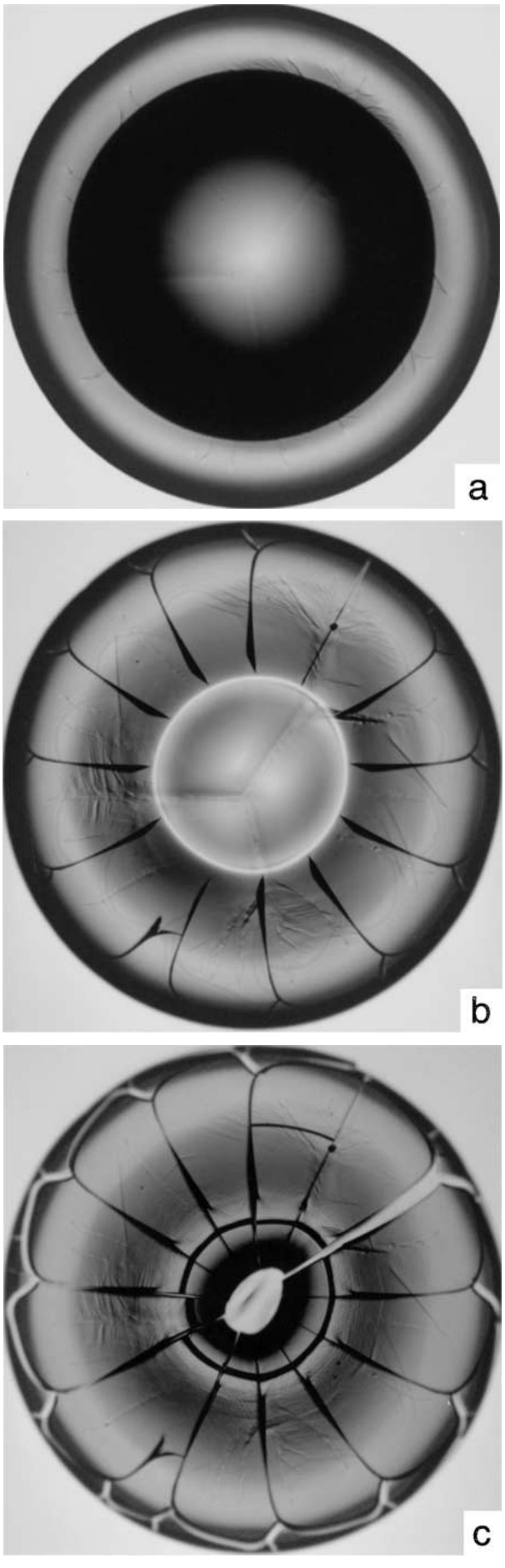

Figure 5 Cracking sequence during rapid drying at 20°C: (a) formation of a rim or foot of gel surrounding liquid sol, (b) radial cracks in gel extending to gel-sol boundary, (c) fully cracked drop with radial and circumferential cracks.

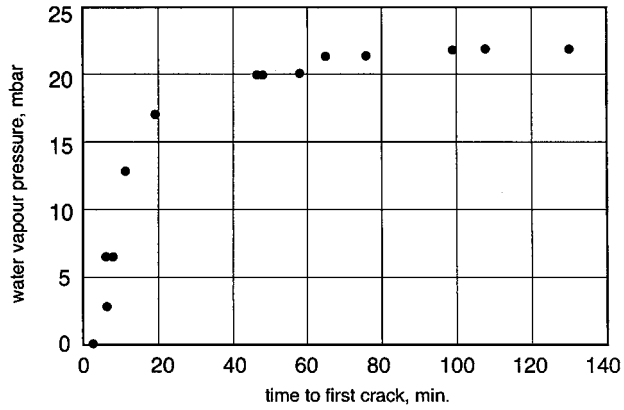

Figure 6 Effect of humidity on time to formation of first cracks.

processes are also influenced by temperature. However, in the range 20 ± 2°C used in this study, only small variations were observed.

3.2. Effect of drying rate on cracking patterns

As mentioned earlier, many processes involving evaporation, diffusion and flow occur during drying. It was found that the relative rates of these processes influence the effects that occur during drying. To illustrate the range of effects that occur we give a detailed account of the processes that were observed in a cell with a nominal equilibrium vapour pressure of 3 to 7 mbar. This is followed by outline details of the effects that were observed when the humidity was increased.

3.2.1. Drying sequence with vapour pressure 3–7 mbar (sulphuric acid concentration 65 to 53%)

The main events that occurred during drying are illustrated by the photographs in Fig. 7 and the schematic drawings of sections through the drying drop in Fig. 8. Initially, a rim of gel formed on the outside of the drop and grew wider. The central region of sol retained the shape of a spherical cap (Fig. 7a–c). Sets of curvilinear orthogonal lines appeared in the gel and grew as the width of the rim increased. These lines are interpreted as shear deformation, associated with shear bands that resulted from in-plane tensile shrinkage stresses in the gel relieved, in part, by deformation. Eventually the sol region transformed completely to gel leaving a small shrinkage hole in the centre (Fig. 7d). For drying under these conditions this stage occurred before the onset of cracking, whereas, in very fast drying, cracking occurred before the transformation to gel was complete (Fig. 5).

Cracking occurred a few seconds after hole formation in 5 to 6 min. The pattern of cracks, which is shown Fig. 7e, formed almost instantaneously but it was possible to follow the sequence. The two primary cracks, that divide the drop into two parts, formed first and were nucleated at the rim of the drop. The secondary cracks then spread around the drop successively forming a series of petal-shaped regions. The primary

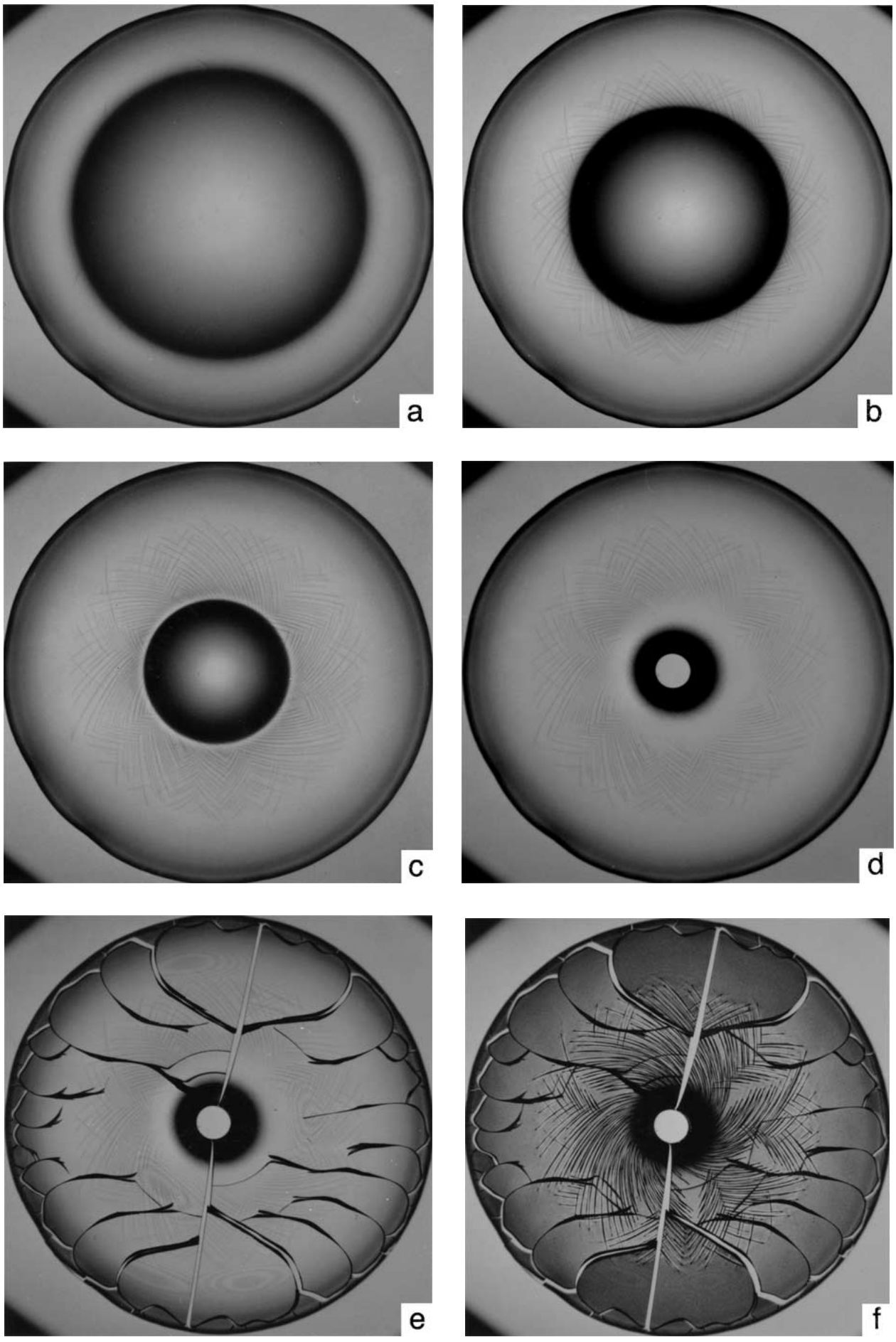

Figure 7 Sequence of changes during drying of a drop in a cell containing 65% H_2SO_4 (equilibrium water vapour pressure 3 mbar). (*Continued*.)

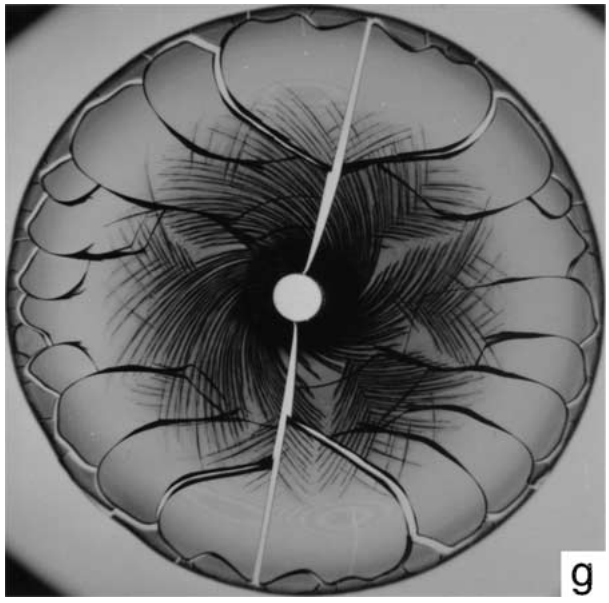

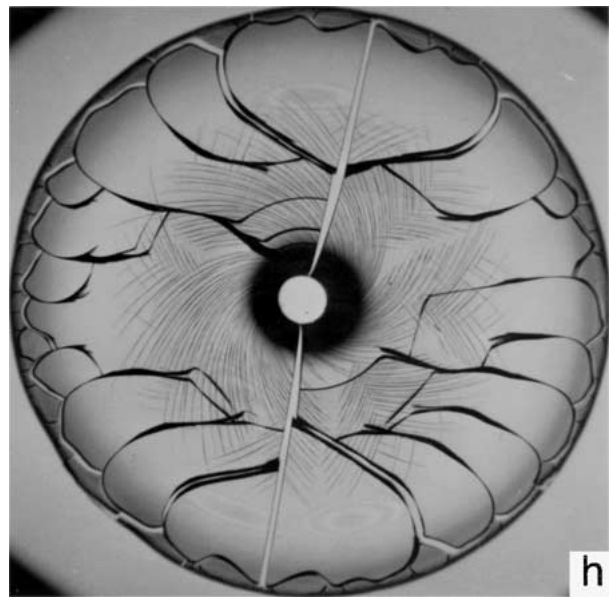

Figure 7 (*Continued*.)

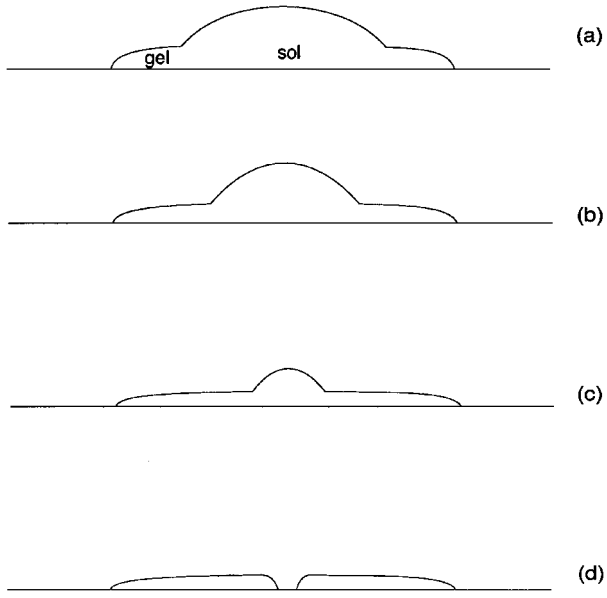

Figure 8 Schematic representation of cross-sectional shape of drop shown in Fig. 7a–d.

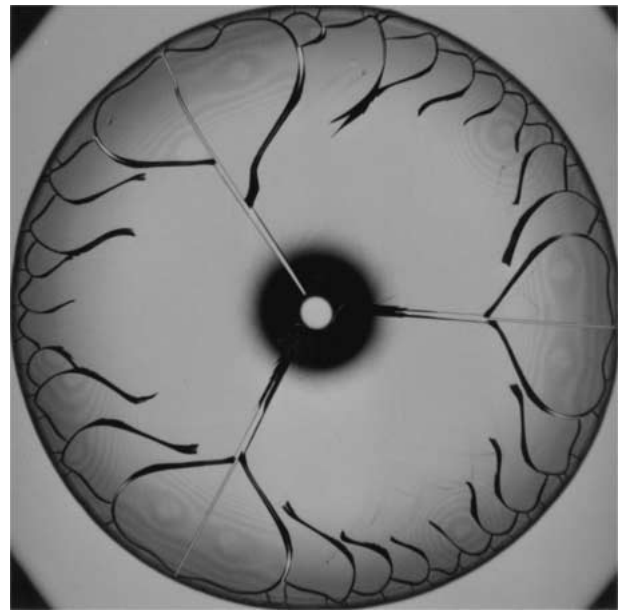

Figure 9 Primary and secondary cracks formed during drying in a cell containing 39% H_2SO_4 (equilibrium water vapour pressure 14 mbar). Interference fringes reveal occurrence of delamination between gel and glass surface.

cracks grew in a radial direction and were at $\pm 45^\circ$ to the shear bands. About 30 s after the completion of cracking the initially transparent drops became clouded and opaque and the shear bands were 'decorated' (Fig. 7f). The clouding disappeared slowly and the decoration of the shear bands became more intense (Fig. 7g). Eventually, the decoration faded and the material became transparent again (Fig. 7h).

3.2.2. Drying sequence with vapour pressure 14 mbar (sulphuric acid concentration 39%)

The changes during drying were similar to those at 3–7 mbar with the development of a rim, progressive growth of shear bands and the formation of a shrinkage hole. However, the time to first cracking was longer and the primary cracking pattern formed as a triplet of radial cracks about $2\pi/3$ apart. This was followed by secondary cracking and delamination (Fig. 9).

3.2.3. Drying sequence with vapour pressure 20 mbar (sulphuric acid concentration 21%)

A small rim with shear bands formed in the early stages. As drying progressed the pattern changed. Wrinkles formed on the surface of the drop. They seemed to occur in a thin skin of gel on the surface of the liquid sol as a result of shrinkage of the skin (Fig. 10a). The wrinkles grew progressively in a radial direction and a small concave region formed in the centre of the drop in the late

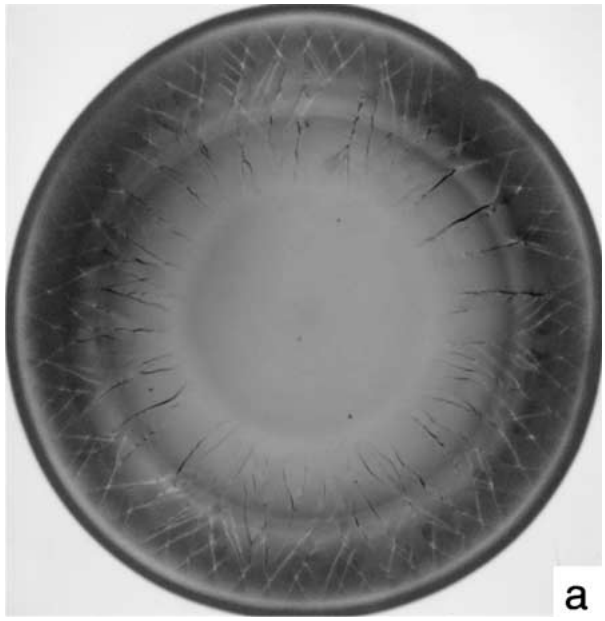

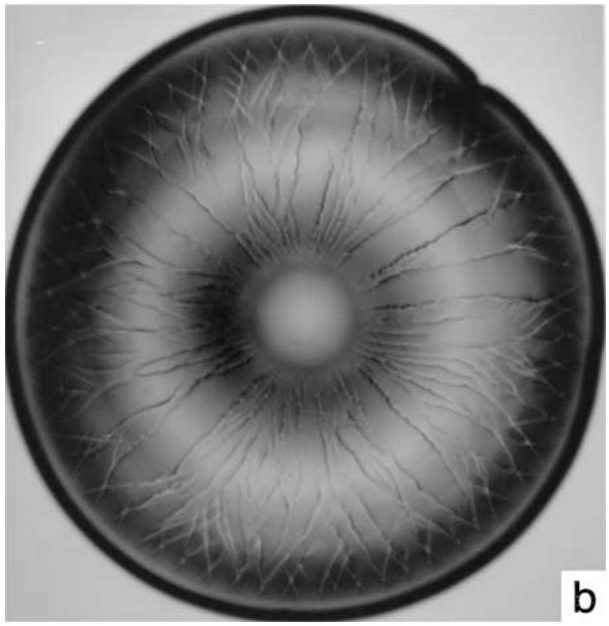

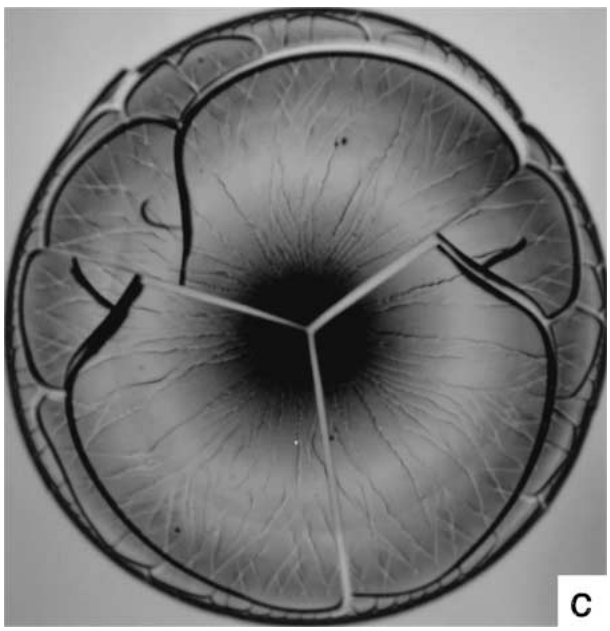

Figure 10 Three stages during drying in a cell containing 21% H_2SO_4 (equilibrium water vapour pressure 22 mbar).

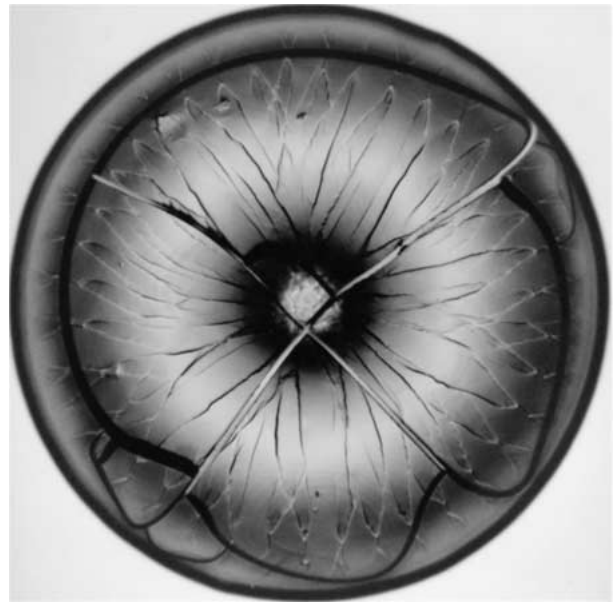

Figure 11 Primary and secondary cracks formed during drying in a cell containing 12% H_2SO_4 (equilibrium water vapour pressure 32 mbar).

stages of drying (Fig. 10b). Primary cracking produced a triplet of radial cracks. Secondary cracks developed slowly and were less numerous than in drops dried in the 39% sulphuric acid cell (Fig. 10c). The secondary cracks followed circular paths close to the edge of the drop.

3.2.4. Drying sequence with vapour pressure 22 mbar (sulphuric acid concentration 12%)

The rim effect was reduced further and a well-developed wrinkle pattern formed. The final cracking pattern consisted of four radial cracks about $\pi/2$ apart and large circumferential cracks (Fig. 11).

3.2.5. Drying sequence with vapour pressure 23 mbar (sulphuric acid concentration 6%)

The radially-oriented pattern of wrinkles formed in the early stages of drying but was eventually replaced in the centre of the drop by a mixture of radial and circumferential wrinkles. Cracking was restricted to a single circumferential crack (Fig. 12) which only occurred after the rate of drying had been increased by slightly heating the cell.

3.3. Miscellaneous experiments to study flow and diffusion during drying

Various dispersions of particles and dyes were added to Ludox TM50 before producing the drops. The drops were then examined, as before, as they dried. The final cracking patterns were largely unaffected by the additions except for small changes associated with dilution.

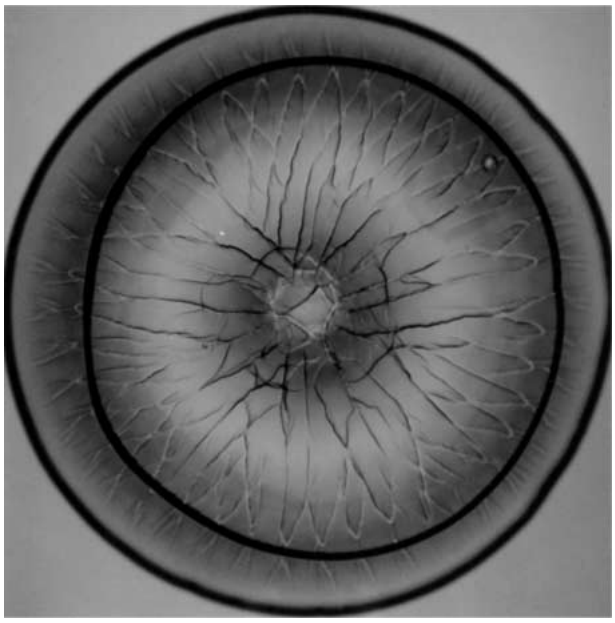

Figure 12 Wrinkles formed during drying in a cell containing 6% H_2SO_4 (equilibrium water vapour pressure 23 mbar). The circumferential crack formed when the temperature of the cell was increased by about 10°C.

3.3.1. Sol containing 0.02% vol colloidal carbon in water

The size of the carbon particles was between 0.5 and 5 μm. Under relatively fast drying conditions (65% sulphuric acid cell) rapid movement of particles occurred in the sol resulting in the aggregation of the particles into large clusters in the centre of the drop. In slow drying conditions (15% sulphuric acid cell) the distribution of particles remained more uniform. Small clusters formed and were aligned in radial directions along the dominant lines of flow in the sol. Differential focussing suggested that flow was outwards close to the upper surface of the drop and inwards on the lower surface.

3.3.2. Sol containing 0.1 wt% fluorescein, a yellow dye

Before the start of drying the dye was uniformly distributed in the sol. The colour appeared denser in the centre because of the spherical-cap shape of the drops. With fast drying the colour rapidly became concentrated in the rim or foot of the drop corresponding to the region that had gelled. The density of dye continued to increase even after the sol had transformed to gel. These effects were much less pronounced in slow drying conditions. When a drop was partially dried under fast drying conditions and then transferred to a cell with a more humid environment to stop the drying process the dye in the outer rim dispersed and the density became uniform throughout the drop. This reverse diffusion of the dye occurred even when the drying sequence was stopped after cracking of the gel had occurred.

4. Discussion

The results demonstrate that the rate of drying has a major influence on the cracking patterns that develop when drops of liquid sol transform by drying to semi-rigid and rigid gels. The times to first cracking increase as the humidity increases and at high humidity cracking does not occur because equilibrium conditions are achieved in the cell. Thus only partial transformation to gel occurs. The experimental observations show that many time dependent processes are involved in the drying process. It is these processes that influence the sequence of events that occur during drying, and the way that internal stresses develop in the drops leading to cracking.

Providing the effects of gravity are ignored the initial shape of the drop of liquid sol on the glass slide (see Fig. 2d) is a spherical cap and is described by the following equations [4].

$$V_{R,\theta} = \pi R^3(2 - 3\cos\theta + \cos^3\theta)/3\sin^3\theta \quad (3)$$

$$V_{R,h} = \pi h(3R^2 + h^2)/6 \quad (4)$$

$$V_{\theta,h} = \pi h^3[1/(1 - \cos\theta) - 1/3] \quad (5)$$

Where V is the volume of the drop and R, h and θ are as illustrated in Fig. 1. The relation between the contact radius, R, the radius of curvature of the free surface of the drop, r, and the contact angle, θ, is

$$R = r\sin\theta \quad (6)$$

The experimental observations on the relation between V, R and θ were consistent with equation 3. Thus, it was found experimentally that a measured volume $V = 1.9$ μl produced a drop on the glass slide with a contact radius $R = 1.7$ mm. For these values Equation 3 predicts a contact angle of $\theta = 27°$ which compares favourably with the measured value of $29+/-2°$. For this drop the calculated height of the drop, $h = 0.4$ mm and $r = 3.7$ mm.

The rate of drying has a strong influence on the distribution of sol and gel in the drop. At all drying rates gel formation occurs initially at the rim of the drop and this leads to pinning of the rim by the solid material. Rapid drying produces the characteristic shape, with a rim of gel surrounding the liquid sol, as described by Parisse and Allain [7] (Fig. 2d). This is a direct result of the rapid loss of water by evaporation from the rim that is greater than the rate of transport by flow and diffusion of water from the centre of the drop. Evidence for these transport effects have been discussed by Deegan *et al.* [6] and are consistent with the experiments with dissolved dyes described earlier. The dyes act as a tracer for the flow of water and it was found that during rapid drying the dye became concentrated at the rim of the drop.

In contrast, during slow drying the rate of loss of water by evaporation is comparable to the rate of transport of water, by diffusion and flow through the sol and gel, so that drying is more uniform. A skin of gel forms over the surface of the drop and the sharp gradients of water concentration evident in rapid drying do not occur. This is most clearly demonstrated by the absence of a central shrinkage cavity in slowly dried drops. In the dye experiments it was found that the distribution

of dye was much more uniform than in the fast drying experiments.

The shrinkage of the sol and the gel that accompanies drying is accommodated in different ways. The total shrinkage associated with complete transformation of the sol to a fully dried rigid gel is about 70% [8]. Constraints to shrinkage depend on the extent of the transformation from sol to gel, the distribution of sol and gel in the drop, and the bonding of the gel to the glass surface. Shrinkage in the liquid state occurs without constraint, other than surface tension forces and the pinning of the rim of the drop to the glass. Thus, at intermediate stages of drying, where the rigid foot surrounds the liquid core, as in Fig. 2d, the dominant constraints associated with shrinkage are circumferential because the gel-sol boundary is stress free. At high rates of drying this leads to the shrinkage cavity in the centre of the drop (see Fig. 7).

Two main deformation mechanisms, associated with shrinkage of the partially gelled material, have been identified. In the early stages of drying the outer rim deforms by shear. The orientation of the shear bands (Fig. 7) indicates that the dominant stresses are tensile in a circumferential direction. Shear deformation dominates in the 'foot' region throughout the drying process for fast drying rates. At slow rates a skin of partially gelled material develops over the dome-shaped drop. Further shrinkage of the underlying sol results in the progressive collapse of the thin skin on the dome and the formation of wrinkles in the skin oriented primarily in radial directions (Fig. 10). The pattern of wrinkles varies somewhat with drying rate presumably because the mode of collapse of the skin depends on the shape of the dome and the distribution of thickness of the skin.

Cracking occurs in the later stages of drying. The results in Fig. 6 show that the time to first cracking is strongly dependent on the water vapour pressure in the cell. It is difficult to make direct comparisons between the data points because drying is not occuring under equilibrium conditions. The relative insensitivity of the time to first cracking to the nominal equilibrium water vapour pressure at short times is probably associated with the delay in achieving equilibrium after the drops are placed in the cell. For equilibrium water vapour pressures exceeding about 18 mbar the time to first cracking increases rapidly with only small increases in vapour pressure.

For very fast drying rates cracking initiates in the 'foot' region before transformation to gel is complete in the centre of the drop (Fig. 5). The cracks nucleate at or close to the rim and then grow in radial directions as the central region of sol retreats. In previous work [1] we have shown that this type of cracking is associated with drying from the outside towards the centre. This creates a concentration gradient in the foot of the drop that is analogous to the temperature gradients that develop in molten basaltic rock as it cools and solidifies. Shrinkage associated with either cooling or drying leads to the development of tensile stresses parallel to the isotherms or isoconcentration profiles.

The circular symmetry of the drop of sol on the glass slide leads to iso-concentration profiles parallel to the rim. The associated shrinkage stress increase as the foot dries. Initially these stresses are accommodated by shear deformation. The curvilinear shear bands lie at $\pm 45^\circ$ to the tensile stress. When the primary shrinkage cracks form they propagate normal to the isoconcentration profiles and at 45° to the shear bands (Fig. 7f). The radial cracks remove circumferential tensile stresses that develop in the later stages of drying. The cusp-shaped cracks close to the rim (Figs 5c and 7h) are associated with the nucleation of the radial cracks and relieve local residual radial tensile stresses. As the radial cracks grow debonding occurs between the gel and the glass as evidenced by the fringe contrast that appears in the outer regions of the drying drop (Fig. 9). After debonding no further cracking occurs in the debonded region. The circular crack in the centre of the fast dried drop (Fig. 5c) is a form of secondary cracking resulting from radial stresses that develop after the primary cracks have formed.

Both the primary and secondary cracking patterns change as the rate of drying decreases. Except at the slowest drying rates (Fig. 12) the primary cracks are radial. Two radial cracks are sufficient to relax the circumferential stresses at relatively fast drying rates (Fig. 7). The number of primary cracks increases progressively to four, as the drying rate decreases, and the tendency to form circumferential cracks increases. In the limit circumferential cracking becomes dominant (Fig. 12). These observations are consistent with the view that the cracking patterns are dominated by the presence of concentration gradients. In the drops that have been dried very slowly the concentration gradients are very small and it is the internal shrinkage at the centre of the drop that generates the radial stresses that lead to circumferential cracks.

It is clear that the rate of drying has a profound effect on the way that shrinkage stresses develop and also on the distribution of shrinkage stresses in the drop. A full explanation of these changes requires a detailed model for the many time dependent processes involved in the evaporation and transport of water in the drop. These, in turn, affect the way that the sol to gel transformation progresses throughout the drop. The complexity of the drying process is demonstrated by the observations on the transport of particles and dyes in the sol-gel during drying. We are unable to offer any explanations for the observations, associated with the later stages of drying, on the clouding of the gel and the decoration of shear bands. Presumably they relate to changes in pore size in the gel, and the distribution of water molecules in the pores, that affect the scattering of light. The decoration of shear bands implies that the shear processes have modified the molecular organisation in these regions.

5. Conclusions

1. The development of shrinkage stresses in sessile drops of silica sol-gel during drying is influenced strongly by the rate of drying.

2. Shrinkage results in a variety of deformation and cracking phenomena that depend on the distribution of stresses in the drops.

3. The effects are related to the distribution of sol and gel during drying that depends on the rate of evaporation from curved surfaces and the diffusion and flow of water through the sol and the gel.

4. The cracking and wrinkling patterns observed confirm our earlier view that drying of silica sol-gel provides a useful model for simulating the formation of cracks during the solidification of basaltic lava flows.

References

1. D. HULL and B. D. CADDOCK, *J. Mater. Sci.* **34** (1999) 5707.
2. J. C. MAXWELL, *Scientific Papers* **2** (1890) 636.
3. C. N. PEISS, *J. Appl. Phys.* **65** (1989) 5235.
4. R. A. MERIC and H. Y. ERBIL, *Langmuir* **14** (1998) 1915.
5. L. LEGER and J. F. JOANNY, *Rep. Prog. Physics* **55** (1992) 431.
6. R. D. DEEGAN, O. BAKAJIN, T. F. DUPONT, G. HUBER, S. R. NAGEL and T. A. WITTEN, *Nature* **389** (1997) 827.
7. F. PARISSE and C. ALLAIN, *Langmuir* **13** (1997) 3598.
8. C. J. BRINKER and G. W. SCHERER, "Sol-Gel Science" (Academic Press, San Diego, 1990).

Received 18 August 2000
and accepted 2 October 2001